Temperature-Dependent Halogen-Exchange Activity Studies of Zeolite-Derived Aluminum Trifluoride

Evan K. L. Y. Hajime, James L. Delattre, and Angelica M. Stacy*

Department of Chemistry, University of California, Berkeley, California 94720

Received August 28, 2006. Revised Manuscript Received December 7, 2006

A high-surface-area (190 m^2/g) amorphous aluminum trifluoride material ("plasma-AlF_3") was synthesized by plasma decomposition of zeolite, and its structural and reactivity properties were investigated. High-resolution transmission electron microscopy of plasma-AlF_3 indicates morphological features on the nanometer-scale, whereas temperature-programmed X-ray diffraction is used to determine the phase-transition temperatures of plasma-AlF_3 to β- and α-AlF_3. Halogen-exchange reactivity is studied by temperature-programmed reaction (TPR) techniques using the dismutation of CCl_2F_2 as a model reaction. Plasma-AlF_3 is found to possess an unexpected low-temperature (>315 °C) activity not observed with the well-known halogen-exchange catalyst β-AlF_3. Supporting TPR studies on aluminum trifluoride hydrates are performed to correlate this new activity with an amorphous AlF_3 structure, and a simple Lewis acid model is presented to explain the reactivity data.

Introduction

Global warming and ozone-layer depletion are two major problems affecting our Earth's atmosphere, and although global warming has been of significant concern most recently, the latter is equally dangerous if not addressed in the near future. Halogen exchange (i.e., intra- and intermolecular halogen metathesis) is significant in the formation of chlorofluorocarbons (CFCs) as well as the conversion of ozone-depleting CFCs to more ozone-friendly HFCs. The importance of these reactions is reflected in the increase in fundamental research on heterogeneous fluorination catalysts during the past decade.[1,2] After it was revealed that CFCs could deplete stratospheric ozone,[3] most research efforts have focused on the preparation of new materials that are active halogen-exchange catalysts, the identification of the active species in these materials, and the study of the mechanisms of halogen exchange.

Among the industrial-scale halogen-exchange catalysts, fluorinated γ-alumina is one of the most widely used for the manipulation of halogenated organics because it effectively catalyzes a variety of halogen-exchange reactions and is relatively inexpensive.[4−8] Unfortunately, the use of highly corrosive fluorinating agents and the inherent induction periods associated with the activation of γ-alumina are continuing concerns for industrial application.[9] Alternatively, the use of pure AlF_3 catalysts could mitigate the continuous need for corrosive fluorinating reagents and any induction periods required for activation of the catalyst. However, the catalytically active phases of aluminum trifluoride are metastable (e.g., β-AlF_3) and therefore must be prepared using multistep, low-temperature syntheses.[10,11] Moreover, the surface areas of these fluoride materials are significantly lower than the corresponding oxides, thereby reducing the volume efficiency of the catalyst.

Part of our research has focused on finding improved techniques for the preparation of catalytically active phases of aluminum trifluoride. Rather than approach this problem using the established chimie douce toolset, we set out to develop a new synthetic approach involving low-temperature plasma chemistry. We recognized early on that heterogeneous reactions using a perfluorocompound (PFC) plasma as the fluorinating agent could be useful as a general route for the preparation of solid fluorides from oxides. For example, consider the overall reaction between CF_4 and Al_2O_3 as shown in eq 1

$$Al_2O_3(s) + {}^3/_2CF_4(g) \rightarrow 2AlF_3(s) + {}^3/_2CO_2(g) \qquad (1)$$

For the reaction above, the Gibbs free energy of the reaction is significantly negative (i.e., $\Delta G_f^{\theta} = -553$ kJ/mol), and therefore the reaction should be favorable under standard conditions. However, not reflected in this calculation are the kinetic aspects of the reaction, as an enormous activation

* Corresponding author. E-mail: astacy@berkeley.edu.

(1) Manzer, L. E. *Science* **1990**, *249*, 31−35.
(2) Manzer, L. E.; Rao, V. N. M. Catalytic Synthesis of Chlorofluorocarbon Alternatives. In *Advanced Catalysis*; Academic Press: San Diego, 1993; Vol. 39, pp 329−350.
(3) Molina, M. J.; Rowland, F. S. *Nature* **1974**, *249*, 810.
(4) McVicker, G. B.; Kim, C. J.; Eggert, J. J. *J. Catal.* **1983**, *80*, 315−327.
(5) Hegde, R. I.; Barteau, M. A. *J. Catal.* **1989**, *120*, 387−400.
(6) Skapin, T.; Kemnitz, E. *Catal. Lett.* **1996**, *40*, 241−247.
(7) Saniger, J. M.; Sanchez, N. A.; Flores, J. O. *J. Fluorine Chem.* **1998**, *88*, 117−125.
(8) Kemnitz, E.; Menz, D. H. *Prog. Solid State Chem.* **1998**, *26*, 97−153.
(9) Hess, A.; Kemnitz, E. *J. Catal.* **1994**, *149*, 449−457.
(10) Kemnitz, E.; Winfield, J. M. Fluoride Catalysts: Their Application to Heterogeneous Catalytic Fluorination and Related Processes. In *Advanced Inorganic Fluorides: Synthesis, Characterization and Applications*; Nakajima, T., Tressaud, B., Žemva, B., Eds; Elsevier Science: Amsterdam, 2000.
(11) Shinn, D. B.; Crocket, D. S.; Haendler, H. M. *Inorg. Chem.* **1966**, *5*, 1927.

10.1021/cm062034x CCC: $37.00
Published on Web 01/20/2007

barrier must be overcome in order to activate CF_4, which will not react with α-Al_2O_3 below 800 °C.[12] This activation barrier can be surmounted without the need for high temperatures by ionizing PFCs at low pressures to generate a "cold" plasma environment with reactive fluorine-containing species. This new synthetic reaction pathway allows for reasonably fast reaction rates at relatively low temperatures.

We previously reported that silica-rich zeolites that were fluorinated with an NF_3 plasma yielded amorphous aluminum trifluoride with an unusually high surface area.[13] The fact that substrates in contact with the plasma can be kept at relatively low temperatures (<100 °C) is of central importance, especially if metastable fluoride catalysts are to be successfully prepared. Another characteristic of the plasma fluorination process that compliments this synthetic approach is that the instability of the molecular species within the plasma could be transferred to the catalyst surface in the form of surface-bound radicals or uncoordinated aluminum sites, thus leading to the possibility of enhanced catalytic activity.

In this paper, we report our results on the characterization of the structure and reactivity of NF_3 plasma/zeolite-derived aluminum trifluoride, hereby referred to as "plasma-AlF_3" throughout the remainder of this paper. Using high-resolution transmission electron microscopy (HR-TEM), the unique characteristics of the plasma-AlF_3 nanostructure have been revealed, whereas structural changes associated with the annealing process were investigated using temperature-programmed synchrotron radiation powder diffraction. The halogen-exchange reactivity of plasma-AlF_3 was characterized by temperature-programmed dismutation reaction experiments, and a model to rationalize all of the experimental findings is presented.

Experimental Section

I. Synthesis. *A. Plasma synthesis of AlF_3.* All reactivity studies were performed on zeolite-derived AlF_3 synthesized by plasma decomposition in a homemade inductively coupled tubular reactor described elsewhere.[14] The plasma reactor consists of a radio frequency power generator (ENI OEM-650A) operating at 13.56 MHz with variable power to ignite and sustain the plasma. Approximately 250−300 mg of zeolite H-SSZ-32 ($H_{1.3}[Al_{1.3}Si_{22.7}O_{48}]$; structure type: MTT; Chevron) precursor was placed in the reactor, and 100 W of rf power was then applied for 30−50 min. The reactant gas used was NF_3 (Scott Specialty Gases), with a flow rate of 10 sccm and a constant chamber pressure of 250 mTorr. During the reaction, the gaseous products were monitored continuously at the reactor exit with a Spectra Satellite quadrupole mass spectrometer. After power to the rf generator and the vacuum pump were terminated, the chamber was backfilled with N_2 gas (99.9% purity) to minimize hydration of the products. The reactor was opened and the alumina crucible was quickly covered and transferred to an argon-filled dry box for further handling.

B. Synthesis of β-AlF_3. To properly characterize the halogen-exchange reactivity of plasma-AlF_3, it was necessary to prepare a well-characterized metastable phase, β-AlF_3, for use as a standard. Pure β-AlF_3 was prepared via the thermal decomposition of $(NH_4)_3AlF_6$ (Aldrich), as described in the literature.[11] Briefly, the ammonium hexafluoroaluminate precursor was placed in a covered alumina crucible and heated in a resistance furnace from 25 to 450 °C in 4 h, and then held at 450 °C for an additional 10 h under flowing N_2 before being cooled back to room temperature. The resulting product yielded crystalline β-AlF_3 according to powder X-ray diffraction analysis (PDF no. 84-1672).

II. Characterization. *A. High-Resolution Transmission Electron Microscopy (HR-TEM).* High-resolution images were collected using the Philips CM200 high-resolution transmission electron microscope at the National Center for Electron Microscopy at Lawrence Berkeley National Laboratory. Samples were dispersed directly on a 3 mm holey carbon grid. Spatially resolved elemental analysis (EDX) was performed using a probe area of ~4 nm^2.

B. Attenuated Total Reflectance FTIR (ATR-FTIR). Attenuated total reflectance Fourier transform infrared (ATR-FTIR) spectroscopy was used as a qualitative probe of the surface and subsurface composition and structure of aluminum trifluoride samples. Spectra were obtained using a Nicolet Avatar 360 FTIR spectrometer equipped with an attenuated total reflectance accessory. Powders were placed directly onto the internal reflection element and pressed with a polyethylene plunger to improve the contact between the sample and crystal. Spectra were averaged over 32 scans in the range of 600−4000 cm^{-1} with 4 cm^{-1} resolution.

C. Powder X-ray Diffraction. Routine powder X-ray diffraction analyses were performed using a Siemens D5000 diffractometer equipped with a standard Cu source X-ray tube, graphite monochromator, and scintillation detection counter. Typical operating conditions of voltage and tube current were 45 kV and 35 mA, respectively. Powder samples were well-ground in a mortar and pestle before analysis. Data were typically collected in the range of $5° \leq 2\theta \leq 75°$ with a step size of 0.05° and a count time of 4 s. Phases were identified by comparing the measured powder patterns against the JC-PDF database of powder patterns.

D. Temperature-Programmed Synchrotron X-ray Powder Diffraction. Temperature-programmed synchrotron X-ray powder diffraction data were collected at Beamline X7B of the National Synchrotron Light Source (NSLS) at Brookhaven National. Full circle powder diffraction profiles were collected on an image plate detector mounted perpendicular to the incident beam. Diffraction from a LaB_6 standard was used to determine the tilt angle, sample-to-detector distance, and wavelength ($\lambda = 0.9274$ Å). Temperature-programmed powder diffraction data collection was performed using a heated sapphire capillary (0.8 mm o.d./0.6 mm i.d.) packed with the sample. The capillary was heated using a resistive heating element that ran parallel to the axis of the capillary. The temperature was measured and controlled by a programmable temperature controller equipped with a 0.010 in. diameter thermocouple (Omega) that was placed inside the capillary. Integration of the full circle reflections was performed using the program Fit2d, excluding single-crystal reflections from the sapphire.

E. Reactivity Characterization. The model halogen-exchange reaction used in this study is the dismutation of CCl_2F_2 as shown in eq 2 below

$$5CCl_2F_2 \rightarrow CCl_3F + 3CClF_3 + CCl_4 \qquad (2)$$

Although CF_4 is in theory a possible product in this system, Kemnitz and co-workers[15,16] have consistently demonstrated that CF_4 does

(12) We determined this value by flowing 20 mL/min of CF_4 over α-Al_2O_3 in a thermogravimetric analyzer. Fluorination was monitored by measuring the associated increase in mass as the temperature was ramped to 1000 °C.

(13) Delattre, J. L.; Chupas, P. J.; Grey, C. P.; Stacy, A. M. *J. Am. Chem. Soc.* **2001**, *123*, 5364−5365.

(14) Delattre, J. L.; Friedman, T. L.; Stacy, A. M. *J. Vac. Sci. Technol., B* **1999**, *17*, 2664−2666.

(15) Krahl, T.; Kemnitz, E. *J. Fluorine Chem.* **2006**, *127*, 663−678.

(16) Murthy, J. K.; Gross, U.; Rudiger, S.; Unveren, E.; Unger, W.; Kemnitz, E. *Appl. Catal., A* **2005**, *282*, 85−91.

not form from dismutation of CCl_2F_2 using conventional aluminum fluoride catalysts.

For the purpose of comparison, the activities of plasma-AlF_3 and β-AlF_3 toward halogen exchange were examined using a homemade gas flow reactor (see the Supporting Information). The design was that of a standard flow through reactor, with the CCl_2F_2 reactant gas passing over a heated sample bed. Product gases were analyzed either by a gas chromatograph and or a mass spectrometer at the reactor exit.

All reactions were performed in a heated quartz microreactor (0.9 mm quartz frit). The thermocouple for monitoring the catalyst temperature was inserted into a glass recess near the bed in the microreactor. A vertical clamshell furnace controlled by a LFE 2010 temperature controller was used for heating the sample. Stainless steel tubing was used throughout, with the exception of the quartz reactor where connections to the reactor were made with Cajon glass-to-metal fittings. Controlled flow of the halocarbon reactant gas was maintained by a Brooks 5850E mass flow controller interfaced to a Brooks 5878 control box.

Analysis of the product gases was performed with a Hewlett-Packard 5890A gas chromatograph (GC) equipped with a flame-ionization detector and Hewlett-Packard 3393A Integrator, which was used to record the chromatogram. The GC was also equipped with a nonpolar HP-5 (5% diphenyl, 95% dimethylpolysiloxane) capillary column (L = 30 m, I.D. = 0.53 mm) and a manual gas-sampling valve with a 1 mL sample loop, which allowed the injection of precise volumes of product gas during sampling. Helium (Air Gas, 99.999% purity) was used as the carrier and makeup gas, and was further purified using an AllTech ALL-Pure Helium purifier and AllTech Oxy-Trap. Contaminants were removed from CCl_2F_2 (Melins, ASTI-70 standard grade) by a homemade scrubber consisting of 3 Å molecular sieves (Davidson, Grade 564, 8−12 mesh). Air (Air Gas, zero grade) and H_2 (Air Gas, Ultrahigh purity) were used as received with no additional purification.

A Spectra Satellite residual gas analyzer (RGA) was used for on-line measurement of the gaseous reaction and desorption products during temperature-programmed experiments. All of the tubing from the exit of the quartz microreactor to the RGA was kept at 110−120 °C to prevent condensation of any reaction products, and the mass analyzer was kept at 80 °C. A metering valve was used to moderate the total flow of gas into the RGA. The Satellite RGA system used in this study consists of an electron gun and a quadrupole mass analyzer for the ionization of the sample gas and separation of the ion fragments, respectively, whereas a Faraday cup detector is used to quantify the relative amount of each m/z value. All data from the RGA was recorded on a PC laptop with RGA for Windows software.

For isothermal experiments, approximately 15−20 mg of solid was loaded into the microreactor and preheated from 22 to 390 °C in 1 h under a He flow to remove any adsorbed water and residual adsorbates. The CFC flow was then initiated, and sampling with the gas chromatograph continued for approximately 1 h.

For temperature-programmed reactions, 15−20 mg of solid were packed into the quartz tube microreactor, providing an average bed volume of ∼5 mm^3. A preheat treatment was performed before each run (from 22 to 300 °C in 45 min, and holding at 300 °C for an additional 45 min under a 100 sccm He flow) to remove any adsorbed water and residual adsorbates. Following the preheat, the reactor was cooled to 100 °C after which a mixed 3:1 He:CCl_2F_2 total flow rate of 100 sccm was established, given an average residence time of 0.9 s. The temperature was then ramped at a constant rate of 7.5 °C/min from 100 to 700 °C, and the gaseous products were monitored using the residual gas analyzer. Commercial $AlF_3 \cdot H_2O$ (Aldrich) was used as a standard in the corresponding TPR-CCl_2F_2 experiments.

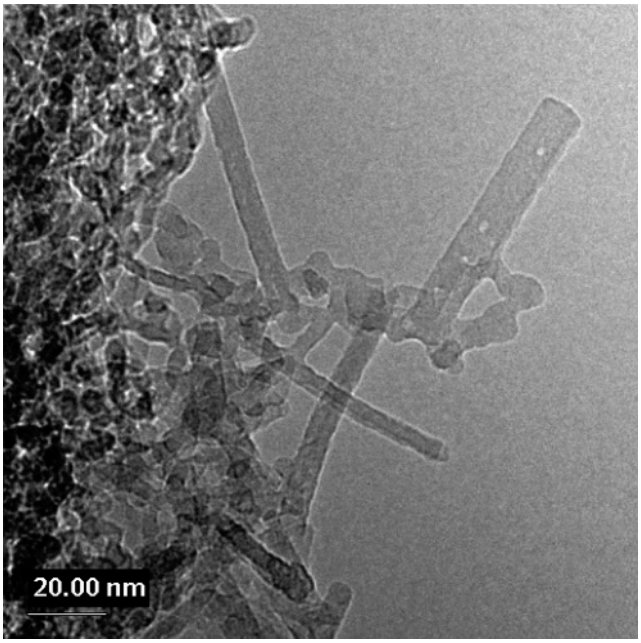

Figure 1. HRTEM image of rodlike nanostructures of plasma-AlF_3.

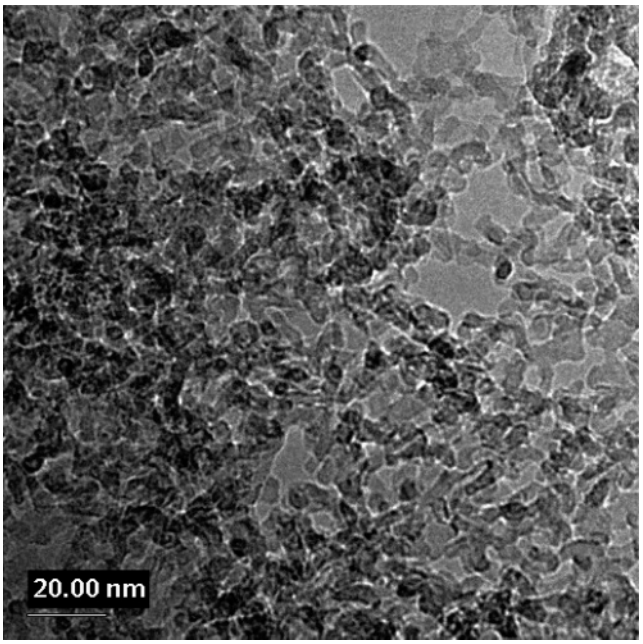

Figure 2. HRTEM image of agglomerated nanoparticles of plasma-AlF_3.

Results and Discussion

I. Structural Characterization. *A. High-Resolution TEM.* High-resolution TEM imaging of plasma-AlF_3 revealed two distinct types of nanostructures. The rodlike structures, shown in Figure 1, are on the order of 20−50 nm in length, whereas the more prevalent structures are smaller 3−5 nm agglomerated particles, shown in Figure 2. Selected area elemental analysis (EDX) showed that both morphologies had the same composition and were comprised of aluminum and fluorine, with a minor oxygen component. The presence of oxygen was likely a result of surface hydration that occurred while loading the sample into the HRTEM. The existence of two

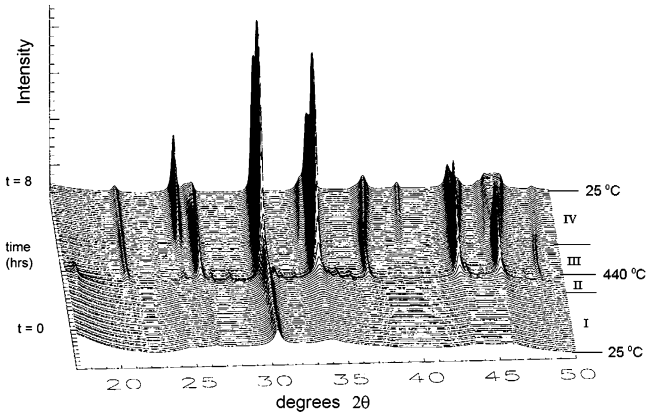

Figure 3. Temperature-programmed, time-resolved synchrotron X-ray diffraction plot of plasma-AlF_3. The sample temperature was ramped from 25 (foreground) to 490 °C over 4 h and then cooled back to 25 °C over a second 4 h interval. The analysis of the plot is summarized in Table 1.

distinct nanostructures with the same composition suggests that there may be two or more distinct crystal growth mechanisms within the plasma environment.

The formation of rodlike nanomorphologies was unexpected, and understanding the precise origin of these features requires further investigation. One possible origin is in the anisotropic etch mechanisms that exist at the plasma−surface interface, thereby inducing a one-dimensional bias into the resulting decomposition product. Another possibility is that the rod formation may be due to crystalline hydrate formation, as will be discussed in a later section.

B. Temperature-Programmed Synchrotron XRD. Halogen-exchange reactions over aluminum fluoride catalysts are typically run at temperatures greater than 300 °C, so it is useful to develop an understanding of the thermal stability of a new catalyst such as plasma-AlF_3. Accordingly, temperature-programmed synchrotron X-ray diffraction (λ = 0.9274 Å) of plasma-AlF_3 was performed at the National Synchrotron Lightsource in order to elucidate information on the structural changes associated with annealing. A time-resolved diffraction plot recorded during a programmed temperature sequence is shown in Figure 3. A capillary packed with plasma-AlF_3 was heated from 25 to 490 °C over 4 h (∼2 °C/min.) and then cooled back to 25 °C over a second 4 h interval. Diffraction patterns were recorded every 5 min 22 s.

The time-resolved plot shown in Figure 3 can be divided into four distinct regions, each with an associated time and temperature range. The boundaries of the regions are demarcated by the appearance or disappearance of reflections that accompany a phase transition. Region I is in the foreground of the plot with a temperature range from 25 to 330 °C. There are very few reflections in this region, which is a consequence of the nearly amorphous nature of plasma-AlF_3, as also evidenced by solid-state NMR spectroscopy.[13] The only reasonably strong reflection occurs at $2\theta = 30.6°$, which has an associated *d*-spacing of 1.76 Å. This distance equals the length of an Al−F bond and we can therefore assume that the structure of plasma-AlF_3 has some medium- to long-range ordering derived from a network of F−Al−F linkages. The reflection at $2\theta = 30.6°$, like the other broad, low-intensity reflections observed in this temperature range, cannot be unequivocally assigned to any one phase of AlF_3 but can be assigned to a number of phases, including both α-and β-AlF_3.

Table 1. Regions of the Time-Resolved, Temperature-Programmed Synchrotron X-ray Diffraction Pattern of Plasma-AlF3 (as shown in Figure 3) and the Phases Observed in Each Region

region	temperature range (°C)	phases
I	25−330	amorphous
II	330−440	β-AlF_3/ cubic-AlF_3
III	440−490	cubic-AlF_3
	490−420	
IV	420−25	α-AlF_3

Region II ranges from 330 to 440 °C. A collection of reflections begin to appear at ∼330 °C that signify the onset of crystallization in the nearly amorphous AlF_3 product. A number of the minor reflections then disappear at 440 °C, with the reflection at $2\theta = 17.8°$ being the clearest example of these transient reflections. Of the reflections that disappear at 440 °C, nine of them can be unambiguously assigned to β-AlF_3, an indication that a fraction of the plasma-AlF_3 product crystallizes as metastable β-AlF_3 upon annealing. Thus, Region II is the temperature range in which small amounts of β-AlF_3 are stable within the annealed product.

Above 440 °C, β-AlF_3 converts to the known high-temperature phase of AlF_3, which has the cubic ReO_3 structure.[17,18] This transition temperature is lower than the reported transition temperatures for bulk β-AlF_3, which have been reported to occur at temperatures ranging from 500 to 730 °C.[9,11,19] The high-temperature cubic phase is represented by several reflections (i.e., $2\theta = 26.2$, 30.6, 33.9, 43.5, and 46.2°) that become very intense at temperatures above 330 °C and remain as the dominant reflections in the powder pattern at temperatures above 440 °C. The reflections from the cubic phase persist through Region III, which extends from 440 to 420 °C on the cooling side of the plot.

Region IV is the remaining cooling portion from 420 to 25 °C. A number of intense reflections (e.g., $2\theta = 43.5$ and 46.2°) from the cubic, high-temperature phase split into multiple reflections upon cooling. The splitting of these reflections is a consequence of the lowering of symmetry that occurs when the high-temperature cubic phase undergoes the rhombohedral distortion to low temperature α-AlF_3. The cubic AlF_3 to α-AlF_3 transition temperature observed here at 420 °C is in reasonable agreement with the literature value of 446 °C that was determined from an AlF_3 single crystal.[18] Table 1 summarizes the phases of AlF_3 observed for each region.

To reiterate the results of Figure 3, upon plasma-AlF_3 being heated, the amorphous AlF_3 structure first partially crystallizes into a mixture of metastable β-phase and high-temperature cubic α-phase at 330−440 °C before completely converting to the high-temperature cubic α-phase above 440 °C. The results described here will take on added significance in the following sections, as they correlate with

(17) Daniel, P.; Bulou, A.; Rousseau, M.; Nouet, J.; Fourquet, J. L.; Leblanc, M.; Burriel, R. *J. Phys.: Condens. Matter* **1990**, *2*, 5663−5677.
(18) Ravez, J.; Mogusmilankovic, A.; Chaminade, J. P.; Hagenmuller, P. *Mater. Res. Bull.* **1984**, *19*, 1311−1316.
(19) Lebail, A.; Jacoboni, C.; Leblanc, M.; Depape, R.; Duroy, H.; Fourquet, J. L. *J. Solid State Chem.* **1988**, *77*, 96−101.

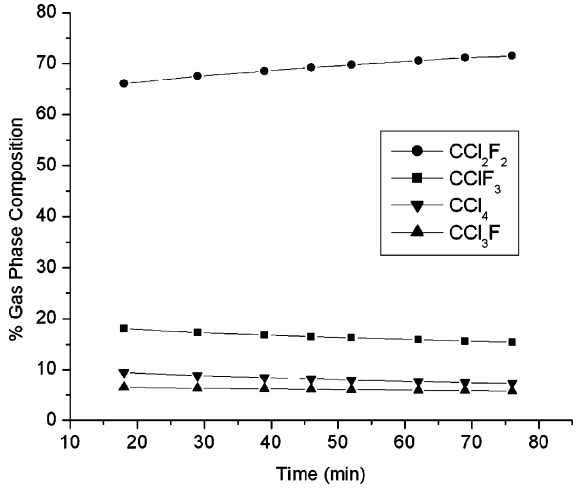

Figure 4. Dismutation of CCl_2F_2 over plasma-AlF_3 at 390 °C.

observations made while characterizing the surface chemistry of plasma-AlF_3.

II. Reactivity Characterization. Structure−reactivity studies of fluorinated alumina and aluminum fluoride materials continue to be a strong area of interest in heterogeneous catalysis, with the discovery of high-surface-area fluorides[20] and theoretical surface structure studies[21] highlighting the most recent progress. In the fluorinated alumina systems, X-ray photoelectron spectroscopy (XPS) studies of γ-alumina pretreated with CHF_3 at 400 °C suggest that an amorphous form of AlF_3 that is structurally similar to β-AlF_3 is the active catalyst.[22] This result is in general agreement with the high level of halogen-exchange activity associated with the pretreatment of γ-alumina with $CHClF_2$ at 500 °C, where the formation of β-AlF_3 was detected by XRD.[23]

Hess and Kemnitz determined that pure β-AlF_3 is catalytically active as synthesized, as opposed to alumina, which requires an induction period.[9] It was also confirmed that the thermodynamically stable α-AlF_3 phase prepared by conventional methods was not active, though both phases are composed of networks of AlF_6 octahedra. The contrast in reactivity observed for β-AlF_3 and α-AlF_3, in spite of their local structural similarities, is undoubtedly due to differences in surface structures of the respective phases that arise due to the different bulk structure. The importance of structure on the halogen-exchange reactivity is strongly evident in the most recent reports of Kemnitz[20] and Harrison,[21] and the following results and discussion on the halogen-exchange behavior of plasma-AlF_3 attempt to further support the structure−reactivity models currently proposed for aluminum fluoride.

A. Isothermal Dismutation Reactivity. The model halogen-exchange reaction used in this study was the dismutation of dichlorodifluoromethane, CCl_2F_2, and is described in more detail in the Experimental Section of this paper. Figure 4 shows a plot of the detected products as a function of time for a typical CCl_2F_2 dismutation reaction experiment at 390 °C with plasma-AlF_3 as the catalyst. The flow of CCl_2F_2 was initiated at $t = 0$ min; after 8 min, unreacted CCl_2F_2 and three distinct product gases were detected. After 18 min, steady-state conditions were reached with the major component of the gas flow being unreacted CCl_2F_2 ($\sim$ 67% conversion). The most intense product peak was assigned to $CClF_3$, with the remaining products, CCl_3F and CCl_4, being detected at lower concentrations. The overall product distribution fits well with the well-established dismutation of CCl_2F_2 (eq 2) observed with other aluminum-fluoride-based materials.[15,16] These results confirm that plasma-AlF_3 is an active halogen-exchange material, producing the expected product gases at relatively constant amounts over an extended period of time.

The reaction conditions were not optimized to give high yields, as this was not the focus of our study. Rather than focusing on the optimization, we use this dismutation reaction to further probe the reactivity of plasma-AlF_3 as a function of temperature in order to gain a better understanding of the relationships between structure and reactivity in this system.

B. TPR−CCl_2F_2: Plasma-AlF_3 versus β-AlF_3. Temperature-programmed reactivity (TPR) studies are valuable surface-characterization experiments as they establish the "thermal window" (i.e., the range of temperatures between the onset of activity and the temperature at which complete conversion to the noncatalytic (α) phase occurs) in which a material can catalyze a reaction. By comparing the TPR profiles of plasma-AlF_3 with that of β-AlF_3, we hoped to gain an understanding of the relative thermal stability of materials, as well as the relative strength of the surface Lewis acid sites.

The TPR plots of plasma-AlF_3 and β-AlF_3 are shown in panels a and b of Figure 5, respectively. The same reactor and reactant gas (i.e., CCl_2F_2) used for isothermal dismutation reactions was employed in the TPR experiments. The temperature was ramped at 7.5 °C/min to 700 °C while the product gases were analyzed using mass spectrometry. Dismutation was monitored by detection of the $m/z = +69$ peak, which corresponds to the most abundant mass fragment of the product $CClF_3$ (i.e., CF_3^+). This peak can be attributed only to the products of halogen exchange and is not detected when there is insufficient thermal energy to initiate the reaction, or when the catalyst has transformed to cubic AlF_3 at higher temperatures.

Comparison of these TPR profiles reveals some significantly different features, most notably the onset of activity of plasma-AlF_3 being shifted to lower temperatures relative to β-AlF_3. Plasma-AlF_3 initiates dismutation of CCl_2F_2 in the range of 315−525 °C, whereas β-AlF_3 is active from 390−700 °C. The observation that plasma-AlF_3 is active at 315 °C, whereas β-AlF_3 does not become active until 390 °C; this suggests that plasma-AlF_3 may possess Lewis acid sites with greater activity than β-AlF_3. It is important to note at this point that the precursor used for β-AlF_3 synthesis was ammonium hexafluoroaluminate and not aluminum fluoride trihydrate ($AlF_3 \cdot 3H_2O$), as is commonly used by Kemnitz et al.[9] The former precursor is found to generate β-AlF_3 that

(20) Kemnitz, E.; Gross, U.; Rudiger, S.; Shekar, C. S. *Angew. Chem., Int. Ed.* **2003**, *42*, 4251−4254.
(21) Wander, A.; Bailey, C. L.; Searle, B. G.; Mukhopadhyay, S.; Harrison, N. M. *Phys. Chem. Chem. Phys.* **2005**, *7*, 3989−3993.
(22) Boese, O.; Unger, W. E. S.; Kemnitz, E.; Schroeder, S. L. M. *Phys. Chem. Chem. Phys.* **2002**, *4*, 2824−2832.
(23) Hess, A.; Kemnitz, E.; Lippitz, A.; Unger, W. E. S.; Menz, D. H. *J. Catal.* **1994**, *148*, 270−280.

exhibits strong dismutation activity as low as 300 °C as opposed to the β-AlF_3 derived from ammonium hexafluoroaluminate used in this study. This distinction has important implications on the interpretation of the reactivity of plasma-AlF_3; for the remainder of this paper, discussion of the reactivity of β-AlF_3 will refer to the fluoroaluminate-derived β-AlF_3 whereas "β-AlF_3 (H_2O)" will refer to β-AlF_3 derived from the trihydrate precursor.

Mechanistically, the lower temperature reactivity of plasma-AlF_3, when compared to β-AlF_3, suggests the presence of unsaturated surface sites on plasma-AlF_3 that are more effective at polarizing the C−X (X = Cl, F) bonds of adsorbed molecules, ultimately lowering the barrier to halogen exchange in a C−X bond-activation model. Recent ab initio density functional theory (DFT) studies on aluminum fluoride surface structures[24] give strong support for the presence of different active Lewis acid sites on crystalline versus amorphous β-AlF_3.

Although plasma-AlF_3 may possess stronger Lewis acid sites, β-AlF_3 clearly maintains greater thermal stability, as this catalyst demonstrates reactivity to 700 °C. This is in agreement with the known thermal properties of β-AlF_3, where the transformation of β-AlF_3 to cubic AlF_3 can be quite slow below 700 °C.[25] One explanation for this difference in thermal stability is that the plasma-AlF_3 network is much less ordered than β-AlF_3 according to our previous XRD and NMR results, and therefore less thermal energy is required to rearrange the atoms and bonds in plasma-AlF_3 into their most thermodynamically stable arrangement (i.e., α-AlF_3). Moreover, the small size of the plasma-AlF_3 nanoparticles may also affect the crystallization temperature, as it is well-known that phase-transition temperatures often decrease with decreasing particle size.[26] On the other hand, the transformation of β-AlF_3 requires the disruption of an extensive, highly crystalline (ordered) network of bonds as an initial step toward the formation of the more stable structure, cubic AlF_3. One would then expect a relatively large kinetic barrier toward the spontaneous transformation of β-AlF_3 to cubic AlF_3.

However, this explanation is flawed when considering the results of Kemnitz et al., in which crystalline β-AlF_3 (H_2O) is found to transform to α-AlF_3 at temperatures above 475 °C.[9] To understand this divergence in thermal stability between β-AlF_3 and plasma-AlF_3, we must therefore consider the thermal stabilities of β-AlF_3 and β-AlF_3 (H_2O) in which the transformation to α-AlF_3 occurs at 700 and 475 °C, respectively. The large difference in thermal stability can be qualitatively rationalized by considering the residual byproducts from thermal decomposition of the corresponding precursors. For β-AlF_3 (H_2O), a minimal amount of H_2O can remain in the product, whereas for β-AlF_3, residual NH_3, HF, or both may remain in the product. These residuals stabilize the β-AlF_3 phase to different extents on the basis of acid−base interactions as well as hydrogen-bonding effects. In both cases, β-AlF_3 would be expected to have greater stability because of the stronger base NH_3 and hydrogen-bonding HF residuals versus H_2O. From this analysis, the absence of NH_3 or HF in plasma-AlF_3 predicts a thermal stability similar to β-AlF_3 (H_2O) (i.e., β to α phase transformation near 475 °C).

C. TPR−CCl_2F_2: Surface Hydration of Plasma-AlF_3. During the course of the structural characterization of plasma-AlF_3, it also became apparent that exposure to the atmosphere altered the properties of the material. The hygroscopic nature of plasma-AlF_3 was evident in the ATR-FTIR spectra of freshly prepared samples (see the Supporting Information), where significant hydration/hydroxylation occurred within minutes of exposure to air. A related Lewis acid catalyst, aluminum chlorofluoride (ACF), demonstrates a similar hygroscopic nature and is reported to deactivate in its reactivity upon exposure to air.[27−29] Another high-surface-area AlF_3 material (HS-AlF_3) synthesized by a sol−gel route also possesses a high sensitivity to moisture, although unlike ACF and plasma-AlF_3, it was found to undergo reversible hydration.[20] To determine if hydration altered the halogen-exchange properties of plasma-AlF_3, we exposed the catalyst to air for varying amounts of time before performing TPR experiments.

Figure 5a shows the TPR profile of a sample that has not been exposed to air. Two other samples were prepared and tested under the same conditions, but were exposed to the laboratory atmosphere for 5 and 17 min prior to the TPR experiments. The TPR profiles for these two samples are shown in Figures 6 and 7, respectively. The hydration of plasma-AlF_3 reveals a complexity in the surface chemistry that was not apparent from Figure 5a alone. The major alteration that occurs upon hydration is the loss of activity in the 315−390 °C range. The degree of deactivation in this region correlates with the exposure time. In comparing Figure 6 to Figure 5a, it is clear that exposure of plasma-AlF_3 to air for 5 min decreases the activity in the 315−390 °C region by approximately one-third. If samples are exposed to air for an additional 12 min (Figure 7), the activity in this temperature range decreases further.

On the other hand, although plasma-AlF_3 is partially deactivated upon exposure to air, we still observe a sharp increase in reactivity at ∼400 °C. As this is the same onset temperature observed for β-AlF_3 in Figure 5b, it is likely that the reactivity observed above 400 °C originates from a different set of Lewis acid sites representative of crystalline β-AlF_3, as suggested earlier. Distinct reflections for β-AlF_3 were observed in the temperature-programmed synchrotron powder pattern for plasma-AlF_3 (Figure 3) and therefore give support to the involvement of β-AlF_3 in the reactivity of plasma-AlF_3. Further discussion on this result is presented in section E.

D. TPR−CCl_2F_2: Plasma-AlF_3 versus AlF_3·$3H_2O$. Over an extended period of time (several days) in air, plasma-

(24) Wander, A.; Bailey, C. L.; Mukhopadhyay, S.; Searle, B. G.; Harrison, N. M. *J. Mater. Chem.* **2006**, *16*, 1906−1910.
(25) Alonso, C.; Morato, A.; Medina, F.; Guirado, F.; Cesteros, Y.; Salagre, P.; Sueiras, J. E.; Terrado, R.; Giralt, A. *Chem. Mater.* **2000**, *12*, 1148−1155.
(26) Andrievski, R. A. *J. Mater. Sci.* **2003**, *38*, 1367−1375.
(27) Krespan, C. G.; Dixon, D. A. *J. Fluorine Chem.* **1996**, *77*, 117−126.
(28) Petrov, V. A.; Krespan, C. G.; Smart, B. E. *J. Fluorine Chem.* **1996**, *77*, 139−142.
(29) Sievert, A. C.; Weigert, F. G.; Krespan, C.G. U.S. Patent 5 157 171, 1992.

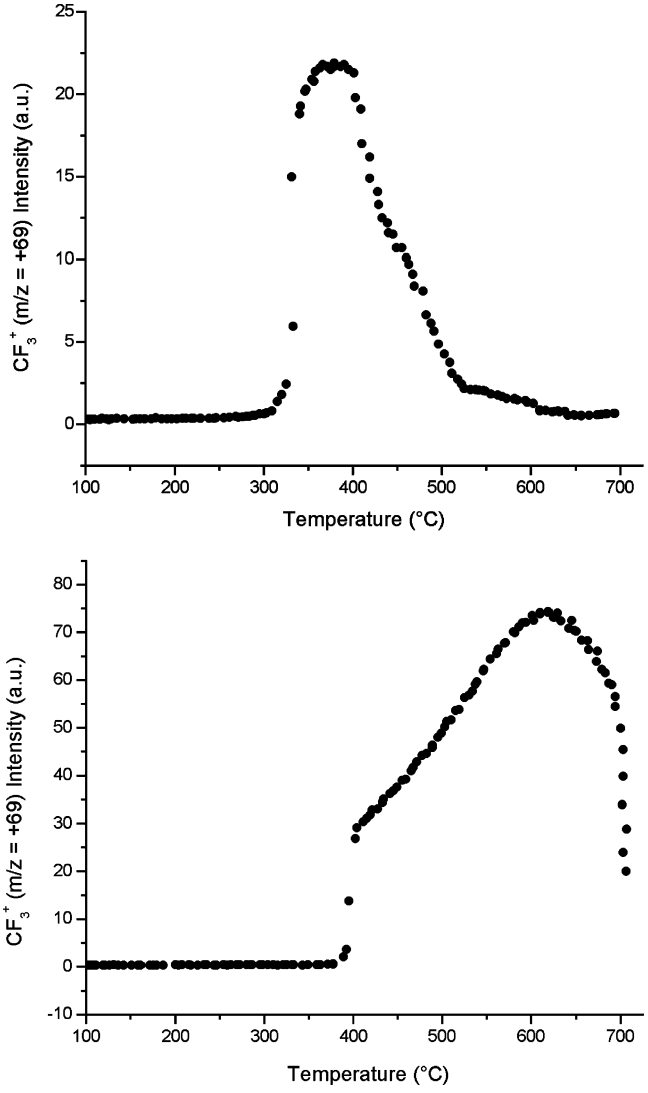

Figure 5. (a) Temperature-programmed reaction of CCl_2F_2 over plasma-AlF_3 with a ramp rate of 7.5 °C/min. The production of $CClF_3$ is determined by measuring the intensity of the CF_3^+ ion by mass spectrometry. (b) Temperature-programmed reaction of CCl_2F_2 over β-AlF_3 with a ramp rate of 7.5 °C/min.

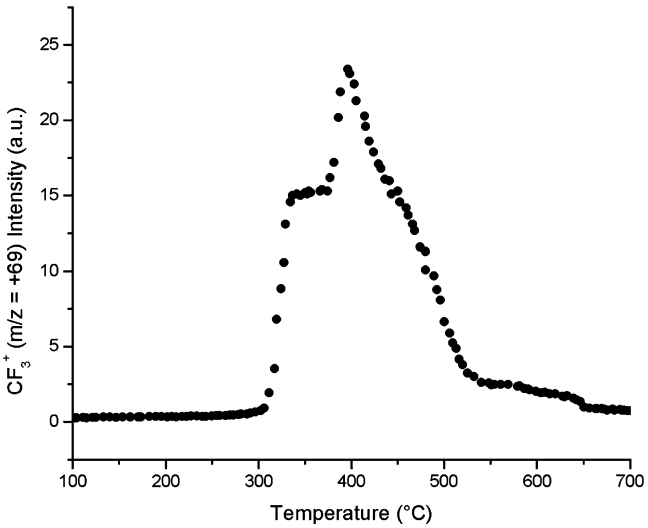

Figure 6. Temperature-programmed reaction of CCl_2F_2 over plasma-AlF_3 pre-exposed to air for 5 min.

AlF_3 unexpectedly converts to a mixture of solid AlF_3 hydrates as observed by ATR-FTIR and powder XRD. This

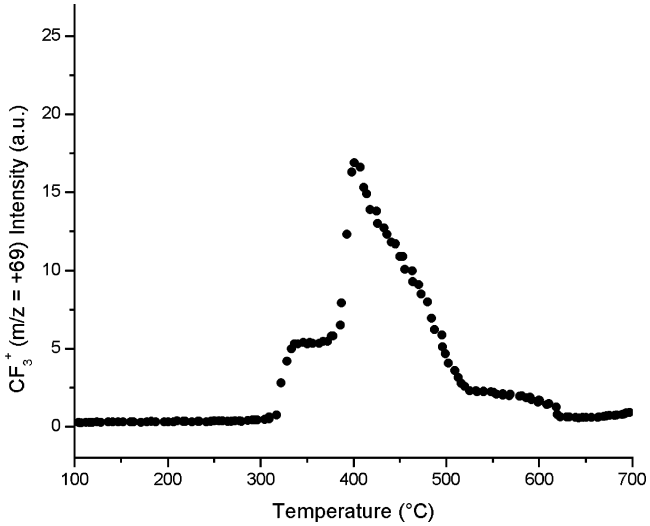

Figure 7. Temperature-programmed reaction of CCl_2F_2 over plasma-AlF_3 pre-exposed to air for 17 min.

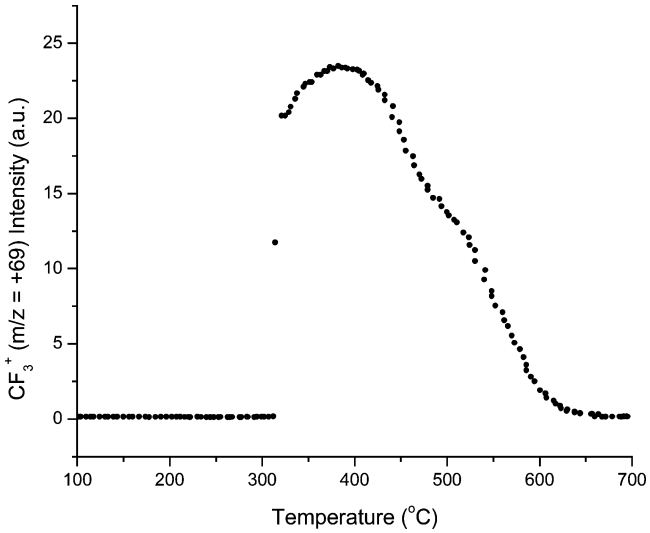

Figure 8. Temperature-programmed reaction of CCl_2F_2 over commercial $AlF_3 \cdot 3H_2O$.

strong affinity for solid AlF_3 to form crystalline hydrates upon exposure to air is not well documented in the AlF_3 literature except in passing.[30] Given the relatively labile nature of H_2O toward Al^{3+} cation[31] versus the fluoride anion and the tendency of plasma-AlF_3 to readily form a hydrate, it would seem that plasma-AlF_3 maintains a deficiency of competing fluoride ligands making up the solid, and suggests the presence of a correspondingly large number of active, coordinatively unsaturated Al sites. The tendency of plasma-AlF_3 to form solid hydrates so readily in air prompted the use of crystalline $AlF_3 \cdot 3H_2O$ as a model compound for the study of hydrated plasma-AlF_3.

As shown in Figure 8, the TPR data for commercial $AlF_3 \cdot 3H_2O$ is similar to the reactivity of "anhydrous" plasma-AlF_3 (Figure 5a), with the onset of reactivity occurring at ~330 °C and no signs of deactivation of the previously proposed low-temperature active sites by water. A closer inspection of the temperature-dependent structural evolution

(30) Scholz, G. *J. Solid State Chem.* **1998**, *139*, 27−36.
(31) Demourgues, A.; Francke, L.; Durand, E.; Tressaud, A. *J. Fluorine Chem.* **2002**, *114*, 229−236.

of $AlF_3 \cdot 3H_2O$ provides an explanation consistent with the observations seen thus far. A classic paper by Le Bail et al.[19] reports the following transformations for the thermal decomposition of $AlF_3 \cdot 3H_2O$

$$AlF_3 \cdot 3H_2O \xrightarrow{220\ ^\circ C} \text{amorphous-}AlF_3 \xrightarrow{450\ ^\circ C} \beta\text{-}AlF_3 \quad (3)$$

From this reaction sequence, an amorphous-AlF_3 material is created in situ upon initial dehydration at 175−220 °C and therefore isolated from any source of water after formation. The dynamic atmosphere present during heating in our TPR experiment is far from the ideal self-generated atmosphere used by Kemnitz,[9] and therefore, highly crystalline β-AlF_3 is not expected below 450 °C. The onset of reactivity at 330 °C would then be assigned to Lewis acid sites that are indicative of a more disordered, amorphous AlF_3 structure, thus explaining the similar low-temperature reactivity to plasma-AlF_3. The loss of activity at lower temperatures for $AlF_3 \cdot 3H_2O$ (∼ 600 °C) compared to β-AlF_3 (∼ 700 °C) can be explained by the arguments given in section B comparing β-AlF_3 and β-AlF_3 (H_2O).

E. Structure−Reactivity Correlations: TPR and TP-XRD. On the basis of the results of the preceding sections, the observed surface reactivity can be correlated with the structure of the plasma-AlF_3 catalyst using currently proposed models of the existence of different types of surface Lewis acid sites. The nonequilibrium condition under which plasma-AlF_3 is prepared creates a disordered network of AlF_6 octahedra with many defects. Surface defects consisting of unsaturated Al centers give rise to Lewis acid sites that are not observed in crystalline β-AlF_3. These Lewis sites catalyze halogen exchange at temperatures as low as 315 °C and, unlike those on β-AlF_3, are deactivated by surface hydration (Figures 6 and 7).

Recently, Harrison and co-workers[24] have reported the theoretical existence of two major types of Lewis acid sites on (100) β-AlF_3 surfaces using ab initio density functional theory. Type 1 sites are true five-coordinate Al sites predicted to exist at crystalline β-AlF_3 surfaces. Type 2 sites consist of two surface Al types: five-coordinate Al sites sharing a fluoride ion and a six-coordinate Al site sharing two fluorides. From the DFT calculations, these higher-energy Type 2 sites are believed to exist only in more disordered AlF_3 structures. Using these descriptors, we can then assign the lower-temperature activity of plasma-AlF_3 (Figures 6 and 7) to a Type 2 active site.

The assignment of Type 2 sites to amorphous, disordered AlF_3 structures has already been proposed to explain the extremely active ACF and HS-AlF_3 prepared by Krespan[27−29] and Kemnitz,[20,32] respectively. On the basis of this reactivity, this would also imply the presence of Type 2 sites in β-AlF_3 (H_2O). The absence of Type 2 sites in β-AlF_3 and presence in β-AlF_3 (H_2O) may be due a disordering effect of water in the latter as opposed to a stabilizing effect of NH_3/HF in the former (as discussed in section B). The effect would create more disordered surface structures in β-AlF_3 (H_2O), giving rise to its lower-temperature activity. In a similar way,

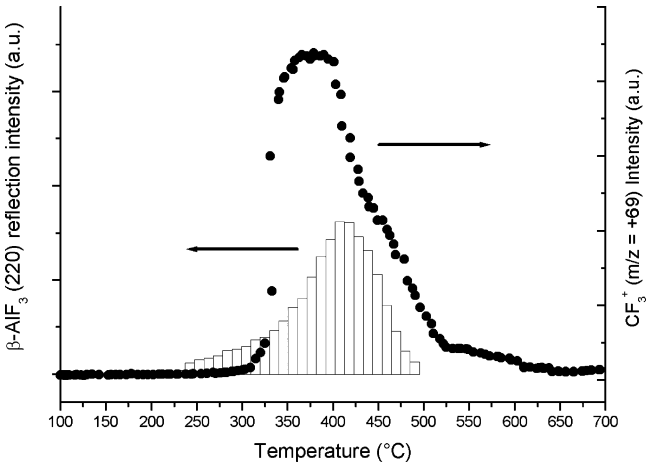

Figure 9. Overlay of TPR plot for plasma-AlF_3 and the corresponding integrated intensity from β-AlF_3 220 reflection in Figure 3.

the presence of organic compounds during the synthesis of ACF is believed to contribute to the large amount of structural disorder in ACF.[15]

As plasma-AlF_3 is heated further, a fraction of the plasma-AlF_3 transforms to crystalline β-AlF_3, with the onset of a higher-temperature reactivity being observed (Figure 6 and 7). A correlation between the existence of β-AlF_3 crystallites and this reactivity is observed by plotting the intensity of the 220 reflection characteristic of β-AlF_3 as observed during temperature-programmed synchrotron diffraction of plasma-AlF_3 (Figure 3) with the TPR profile for plasma-AlF_3 (Figure 5a). This plot, comparing the thermal evolution of the powder XRD data and the reactivity, is shown in Figure 9.

Reflections from β-AlF_3 are observed at temperatures as low as 250 °C, but the intensity of these reflections is minimal until ∼330 °C. β-AlF_3 crystallizes gradually from 330 to 407 °C, where the largest amount of β-AlF_3 is observed in the powder pattern. Interestingly, the β-AlF_3 maximum in the powder pattern coincides with the onset of halogen exchange in traditionally prepared β-AlF_3. As the temperature is increased from 407 to 500 °C, significant amounts of cubic AlF_3 form, whereas the β-AlF_3 reflections and the activity of the catalyst diminish. The observation that the decrease in the β-AlF_3 220 peak intensity correlates well with the decrease in activity suggests that the small amount of β-AlF_3 that forms during annealing plays a role in the observed reactivity in the 400−525 °C range. A very small amount of activity occurs up to ∼630 °C, possibly from β-AlF_3 crystallites that are slow to convert to cubic AlF_3.

This higher-temperature activity may be due to the Type 1 active sites described by Harrison, where the presence of crystalline β-AlF_3 appears to be essential. The higher temperature required for activity at these Type 1 sites may be related to an activation barrier imposed by the strict five-coordinate geometry of the aluminum ion, whereas the lower temperature Type 2 active site would possess a lower activation barrier to reaction due to a more weakly bound, shared fluoride ions, allowing for flexibility in stabilizing higher-energy transition-state geometries. According to Harrison,[21,24] the presence of Type 1 sites should be readily observed by surface core level X-ray spectroscopy, where a

(32) Ruediger, S. K.; Gross, U.; Feist, M.; Prescott, H. A.; Shekar, S. C.; Troyanov, S. I.; Kemnitz, E. *J. Mater. Chem.* **2005**, *15*, 588−597.

very large core level shift of the F 1s binding energy is predicted. However, previous ESCA studies did not reveal the predicted shift nor any major difference in F 1s binding energy between β-AlF_3 (H_2O) and α-AlF_3.[23] Another possible explanation of the higher temperature reactivity may be based on a different Type 2 site that is formed from the increasing input of thermal energy during the TPR experiment. Current work by Harrison et al.[24] on the binding energy of NH_3 to Type 1 and Type 2 sites in correlation with the TPD-NH_3 studies of Kemnitz should help to clarify the assignments of the various surface sites in aluminum fluoride materials.

Amorphous AlF_3 systems offer a new avenue for investigation into the study of halogen-exchange activity. The significance of amorphous AlF_3 as opposed to crystalline β-AlF_3 in halogen-exchange activity has been mentioned in X-ray absorption and photoelectron studies in the past[22] and is more recently supported by an excellent solid-state NMR study by Chupas et al.[33] and the very promising ACF and HS-AlF_3 systems previously mentioned. Kemnitz and coworkers have already expanded the study of disordered aluminum fluorides significantly,[32,34] including an extensive review of ACF[15] and studies of the reactivity of ACF, HS-AlF_3, and amorphous AlF_3 (from thermal decomposition of $AlF_3 \cdot 3H_2O$).[20] In these studies, ACF and HS-AlF_3 were found to possess extraordinarily strong acid sites not observed with amorphous AlF_3 or β-AlF_3 (H_2O). According to our current assignments of Type 2 sites, this would imply that ACF and HS-AlF_3 may possess even higher energy Lewis acid sites not revealed in Harrison's DFT work based on the (100) surface of β-AlF_3. There is a possiblility that starting from another metastable phase of AlF_3 or another plane of β-AlF_3 may produce these higher-energy, more active Lewis acid sites.

Conclusion

More than a decade since the global ban on CFCs, the search for alternatives continues to be an active field of research; in turn, the synthetic routes to these new alternatives are also under constant investigation. Aluminum-trifluoride-based materials remain as a major component in these synthetic schemes for their use in a variety of halogen-exchange reactions and are being modified continually to optimize their halogen-exchange activity. We have recently provided a route to high-surface-area, amorphous AlF_3 through the NF_3-plasma decomposition of zeolite. The halogen-exchange activity of plasma-AlF_3, probed using temperature-programmed dismutation experiments of CCl_2F_2, revealed a low-temperature activity (>325 °C) that is also found in other amorphous AlF_3 materials. It was later found that TPR experiments of commercial $AlF_3 \cdot 3H_2O$ displayed similar reactivity to plasma-AlF_3 and that the similar reactivity between these two AlF_3-based materials most likely arises from the amorphous structures present during the temperature ramp. As a result, the low temperature activity is thought to be a characteristic feature of structurally amorphous AlF_3 originating from coordinately unsaturated Type 2 Lewis acid sites as described by Harrison. However, these Type 2 sites are also believed to be present at disordered surfaces of crystalline β-AlF_3 (H_2O) on the basis of reactivity data.

The formation of β-AlF_3 was observed in the temperature-programmed synchrotron XRD data of plasma-AlF_3. Overlaying the integrated intensity of reflections of β-AlF_3 from the TP-XRD of plasma-AlF_3 and the TPR-CCl_2F_2 data of plasma-AlF_3 shows the correlated emergence of β-AlF_3 with the reactivity profile of plasma-AlF_3. This correlation suggests the existence of a set of distinct Lewis acid surface sites related to crystalline β-AlF_3, although further studies are necessary to elucidate the true identity of these sites.

Acknowledgment. We thank Dr. Melissa S. Sander for assistance with HRTEM imaging, Professor Jeffrey R. Long for use of the ATR-FTIR spectrometer, and Professor Clare P. Grey, Dr. Peter J. Chupas, and Dr. Jonathan C. Hanson for their assistance with the synchrotron XRD experiments. We also thank Robyn Woo and Todd Ostomel for their help in the synthesis of β-AlF_3 and the design and construction of the gas flow reactor. This work was generously supported by the ACF-PRF grant fund. Finally, we would like to express our deepest appreciation to Professor Dr. Erhard Kemnitz for the enormous amount of generosity in both time and suggestions in the writing of this manuscript.

Supporting Information Available: Schematics of the gas-flow reactor (PDF). ATR-FTIR spectra for plasma-AlF_3, hydrated plasma-AlF_3, and commercial $AlF_3 \cdot 3H_2O$ (PDF). Powder XRD pattern for hydrated plasma-AlF_3 (PDF). This material is available free of charge via the Internet at http://pubs.acs.org.

CM062034X

(33) Chupas, P. J.; Corbin, D. R.; Rao, V. N. M.; Hanson, J. C.; Grey, C. P. *J. Phys. Chem. B* **2003**, *107*, 8327−8336.
(34) Krahl, T.; Stosser, R.; Kemnitz, E.; Scholz, G.; Feist, M.; Silly, G.; Buzare, J. Y. *Inorg. Chem.* **2003**, *42*, 6474−6483.